PCCP

PAPER

View Article Online
View Journal

Cite this: DOI: 10.1039/c4cp01787k

Use of heteroaromatic spacers in isoindigo-benzothiadiazole polymers for ambipolar charge transport†

Gyoungsik Kim,‡[a] A-Reum Han,‡[ab] Hae Rang Lee,[b] Joon Hak Oh*[b] and Changduk Yang*[a]

Received 25th April 2014,
Accepted 26th June 2014

DOI: 10.1039/c4cp01787k

www.rsc.org/pccp

Inspired by the outstanding charge-transport characteristics of poly(isoindigo-*alt*-benzothiadiazole) (PIIG-BT) in our previous study, herein we present two new polymers (**PIIG-DTBT** and **PIIG-DSeBT**) involving IIG and BT blocks constructed using five-membered heteroaromatic spacers such as thiophene (T) and selenophene (Se) and investigate the effects of the spacer groups on the optical, electrochemical, and charge-transport properties. As a consequence of the red-shifts induced by the more extended conjugation and enhanced intramolecular charge transfer (ICT), both **PIIG-DTBT** and **PIIG-DSeBT** show smaller bandgaps compared to PIIG-BT. Interestingly, the LUMO energy levels (−3.57 eV) for the two polymers are the same, but the HOMO levels (−5.39 and −5.26 eV for **PIIG-DTBT** and **PIIG-DSeBT**, respectively) clearly vary as a function of the structural modification of the spacers. In addition to the changes in their optical properties and energy levels induced by the incorporation of the spacers, ambipolar charge transport behaviors with hole and electron mobilities of up to 7.8×10^{-2} and 3.4×10^{-2} $cm^2 V^{-1} s^{-1}$, respectively, are observed for **PIIG-DTBT** films with highly ordered lamellar packing. This represents the second example of IIG-based polymers exhibiting ambipolar charge transport in OFETs reported to date.

Introduction

π-Conjugated polymers for organic field-effect transistors (OFETs) have attracted considerable attention because of their easy modification of structure, solution processability, and low-cost device fabrication.[1–13] Owing to its capability to facilitate π–π stacking with a large overlapping area and intermolecular interactions induced by a macromolecular conjugated system involving alternating electron-rich and -deficient substituents, the donor–acceptor (D–A) approach has found its foremost application in the molecular design and synthesis with the goal of improving the charge-carrier mobilities in OFETs.[11–19]

Within the class of D–A materials, the isoindigo (IIG) unit has proven to be one of the most promising acceptor units for high-performance OFET materials. For example, by copolymerizing with numerous electron-rich blocks, great achievements in the resulting IIG-based D–A polymers for OFETs have been made in recent years.[20–26] Some IIG–oligothiophene polymers exhibited hole mobilities exceeding 1.0 $cm^2 V^{-1} s^{-1}$.[24–28] Furthermore, the halogenated IIG-containing polymers pioneered by Pei and co-workers showed excellent ambipolar charge-carrier transport in IIG-based polymers, for the first time.[29] On the other hand, n-type behavior is not universal in IIG-based polymers, limiting their application in n-type OFETs so far. In order to satisfy the demand for comparable performance characteristics for n-type OFETs, very recently our group reported an IIG-based polymer with electron-deficient benzothiadiazole (BT) as another acceptor unit in the polymer backbone, the so-called A–A type, showing unipolar n-type OFET behavior with an electron mobility of up to 0.22 $cm^2 V^{-1} s^{-1}$.[22]

Motivated by this intriguing result, in the present study, we devote our attention to the insertion of heteroaromatic spacer groups in between adjacent IIG and BT units along the backbone, with a view to explore the impact of implanting heteroaromatic spacers into the IIG–BT polymer on the opto-electronic, electrochemical, and carrier-transport properties. Our choice for the heteroaromatic spacers is five-membered heterocyclic units such as thiophene (T) and selenophene (Se) because they can relieve the steric hindrance between the IIG and BT units, hence enhancing co-planarity of the polymer backbone, which would be preferable for charge transport by hopping.[30–32]

[a] School of Energy and Chemical Engineering, Low Dimensional Carbon Materials Center, Ulsan National Institute of Science and Technology (UNIST), Ulsan 689-798, South Korea. E-mail: yang@unist.ac.kr
[b] Department of Chemical Engineering, Pohang University of Science and Technology, Pohang, Gyeongbuk 790-784, South Korea. E-mail: joonhoh@postech.ac.kr

† Electronic supplementary information (ESI) available. See DOI: 10.1039/c4cp01787k

‡ These authors contributed equally.

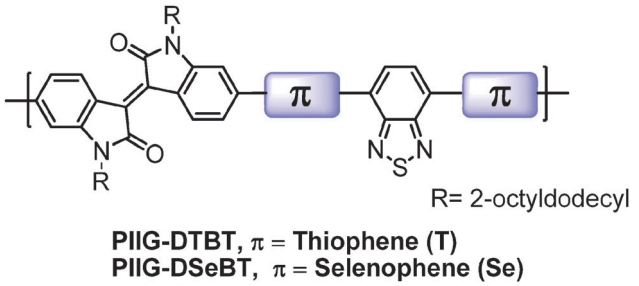

Fig. 1 Molecular structures of **PIIG-DTBT** and **PIIG-DSeBT**.

The chemical structures of the studied polymers (**PIIG-DTBT** and **PIIG-DSeBT**) are shown in Fig. 1. In this study, we present the syntheses, photophysical and electrochemical properties, and OFET performance. More than just tuning the optical properties and energy levels of the IIG–BT parent polymer, the incorporation of the heteroaromatic spacers affects the polarity in OFET devices, eventually leading to relatively well-balanced ambipolar transport behavior that is very rare for IIG-based polymers.

Experimental

Materials and instruments

6,6′-(*N*,*N*′-2-Octyldodecyl)-pinacoldiboronisoindigo (**1**), 4,7-di(5′-bromo-2′-thienyl)-2,1,3-benzothiadiazole (**2**), and 4,7-di(5′-bromo-2′-selenienyl)-2,1,3-benzothiadiazole (**3**) were synthesized according to the literature.[22,33,34] ^{1}H NMR spectra were recorded on a Varian VNRS 600 MHz (Varian USA) spectrophotometer using $CDCl_3$ as solvent and tetramethylsilane (TMS). UV-Vis spectra were recorded on a UV-1800 (SHIMADZU) spectrometer. Number-average (M_n) and weight average (M_w) molecular weights, and polydispersity index (PDI) of the polymer products were determined by gel-permeation chromatography (GPC) using a Perkin-Elmer Series 200 and a series of monodisperse polystyrenes as standards in THF (HPLC grade) at 313 K. Cyclic voltammetry (CV) measurements were performed on an AMETEK VersaSTAT 3 with a three-electrode cell in a nitrogen bubbled 0.1 M tetra-*n*-butylammonium hexafluorophosphate (*n*-Bu_4NPF_6) solution in acetonitrile at a scan rate of 50 mV s^{-1} at room temperature. An Ag/Ag$^+$ (0.1 M of $AgNO_3$ in acetonitrile) electrode, a platinum wire and a polymer coated glassy carbon electrode were used as the reference electrode, counter electrode and working electrode, respectively. The Ag/Ag$^+$ reference electrode was calibrated using a ferrocene/ferrocenium redox couple as an external standard, whose oxidation potential is set at −4.8 eV with respect to the zero vacuum level. The HOMO energy levels were obtained from the equation HOMO = $-(E_{ox}^{onset} - E_{(ferrocene)}^{onset} + 4.8)$ eV. The LUMO levels of polymers were obtained from the equation LUMO = $-(E_{red}^{onset} - E_{(ferrocene)}^{onset} + 4.8)$ eV. Tapping-mode atomic force microscopy (AFM) measurements were performed using an Agilent 5500 scanning probe microscope (SPM) running with a Nanoscope V controller. The Rigaku high power X-ray diffractometer was used (D/MAZX 2500V/PC) to observe out-of-plane molecular packing in polymer films. X-ray diffraction (XRD) patterns were recorded under an X-ray power of 40 kV and a scan rate of 1° min^{-1}.

OFET fabrication and measurement

Bottom-gate top-contact OFET devices based on the spacer containing IIG–BT polymers were fabricated on a highly n-doped Si substrate with a thermally grown 300 nm-thick SiO_2 layer (C_i = 10 nF cm^{-2}), where the highly n-doped Si and SiO_2 layers were used as the gate electrode and dielectric, respectively. The surface of SiO_2/Si wafer was treated with *n*-octadecyltrimethoxysilane (OTS), as reported previously.[15,35] After cleaning the SiO_2/Si wafers with piranha solution (a 7 : 3 mixture of H_2SO_4 and H_2O_2), OTS solution (3 mM in trichloroethylene) was spin-coated on the SiO_2/Si substrate at 3000 rpm for 30 s. The OTS-deposited wafers were exposed to ammonia vapor in a desiccator for 12 h. Then, the wafers were rinsed with toluene, acetone, and isopropyl alcohol. The contact angle (DI water) on the hydrophobic OTS-treated wafers was typically ∼110°. The spacer containing IIG–BT polymers (**PIIG-DTBT** and **PIIG-DSeBT**) were dissolved in anhydrous *o*-dichlorobenzene (∼3 mg mL^{-1}) and the polymer films were prepared on the OTS-treated SiO_2/Si substrates by the drop-casting method. Then, the polymer films were annealed on a hot plate at 220 °C for 30 min under a N_2 atmosphere. Gold electrodes (40 nm) were thermally evaporated through a shadow mask with a channel length (L) of 50 μm and width (W) of 1000 μm. The current–voltage characteristics were measured in a N_2-filled glovebox by using a Keithley 4200 semiconductor parametric analyzer. The field-effect mobility was calculated in the saturation regime using the following equation:

$$I_{DS} = 1/2(W/L)\mu C_i(V_G - V_T)^2$$

where I_{DS} is the drain current, W and L are the semiconductor channel width and length, respectively, μ is the mobility, C_i is the capacitance per unit area of the gate dielectric, and V_G and V_T are the gate voltage and threshold voltage, respectively.

Suzuki-type polymerization

PIIG-DTBT: In a Schlenk flask, 6,6′-(*N*,*N*′-2-octyldodecyl)-pinacoldiboronisoindigo (**1**) (219 mg, 0.204 mmol) and 4,7-di(5′-bromo-2′-thienyl)-2,1,3-benzothiadiazole (**2**) (93 mg, 0.204 mmol) were dissolved in toluene (7 mL), to this a solution of K_3PO_4 (217 mg, 1.02 mmol), tri-*o*-tolylphosphine (3.7 mg, 12.2 μmol) and deionized water (1.5 mL) were added. The mixture was vigorously stirred at room temperature under argon. After 30 min, $Pd_2(dba)_3$ (3.7 mg, 4.08 μmol) was added to the reaction mixture and stirred at 90 °C for 3 d. After that, the solution was precipitated in a mixture of methanol and ammonia (4 : 1 v/v, 250 mL). This was filtered off through a paper filter under vacuum, washed in a Soxhlet apparatus with methanol (1 d), acetone (1 d), hexane (1 d) and chloroform (1 d) to remove the low molecular weight product. Finally, the chlorobenzene fraction was re-precipitated into methanol and filtered off through a 0.45 μm Teflon filter. The polymer was obtained as a chlorobenzene soluble black powder, 73 mg (32%) (M_n = 6.5 × 10^3 g mol^{-1}, PDI = 2.13). ^{1}H NMR (600 MHz, $CDCl_3$) δ (ppm) 9.22–9.20 (br, 2H), 8.16–7.84 (br, 6H), 7.52–6.67 (br, 6H), 3.76–3.50 (br, 4H), 2.11–1.26 (br, 64H), 0.87–0.84 (br, 12H).

Elemental analysis: C, 74.96; H, 8.63; N, 4.99; O, 2.85; S, 8.58. Found: C, 74.7; H, 8.52; N, 4.74; O, 3.24; S, 8.38.

PIIG-DSeBT: In a Schlenk flask, 6,6′-(*N*,*N*′-2-octyldodecyl)-pinacoldiboronisoindigo (**1**) (219 mg, 0.204 mmol) and 4,7-di(5′-bromo-2′-selenienyl)-2,1,3-benzothiadiazole (**3**) (113 mg, 0.204 mmol) were dissolved in toluene (7 mL), to this a solution of K_3PO_4 (217 mg, 1.02 mmol), tri-*o*-tolylphosphine (3.7 mg, 12.2 μmol) and deionized water (1.5 mL) was added. The mixture was vigorously stirred at room temperature under argon. After 30 min, $Pd_2(dba)_3$ (3.7 mg, 4.08 μmol) was added to the reaction mixture and stirred at 90 °C for 3 d. After that, the solution was precipitated in a mixture of methanol and ammonia (4 : 1 v/v, 250 mL). This was filtered off through a paper filter under vacuum, washed in a Soxhlet apparatus with methanol (1 d), acetone (1 d), hexane (1 d), and chloroform (1 d) to remove the low molecular weight product. Finally, the chlorobenzene fraction was re-precipitated into methanol and filtered off through a 0.45 μm Teflon filter. The polymer was obtained as chlorobenzene soluble black powder, 73 mg (32%) (M_n = 1.6 × 10^4 g mol^{-1}, PDI = 3.45). ^{1}H NMR (600 MHz, $CDCl_3$) δ (ppm) 9.17–8.89 (br, 2H), 8.18–6.38 (br, 10H), 3.74–3.49 (br, 4H), 2.10–1.02 (br, 64H), 0.88–0.72 (br, 12H). Elemental analysis: C, 69.17; H, 7.96; N, 4.61; O, 2.63; S, 2.64. Found: C, 68.77; H, 7.66; N, 4.58; O, 2.62; S, 2.59.

Results and discussion

Synthetic approach and characterization

The synthetic routes for preparation of the target polymers (**PIIG-DTBT** and **PIIG-DSeBT**) are outlined in Scheme 1. The key monomers, 6,6′-(*N*,*N*′-2-octyldodecyl)-pinacoldiboronisoindigo (**1**) (three steps: condensation, alkylation, and Miyaura borylation), 4,7-di(5′-bromo-2′-thienyl)-2,1,3-benzothiadiazole (**2**), and 4,7-di(5′-bromo-2′-selenienyl)-2,1,3-benzothiadiazole (**3**) (two steps for each compound: Stille coupling and bromination), were easily synthesized according to the previously reported methods. By copolymerizing the diborylated isoindigo and dibrominated monomers under the Suzuki conditions in degassed toluene/water, using K_3PO_4 as a base, $Pd_2(dba)_3$ as a catalyst, P(*o*-tolyl)$_3$ as the corresponding ligand, the target polymers, *i.e.*, **PIIG-DTBT** and **PIIG-DSeBT**, were obtained, respectively. The purification processes involved precipitation into methanol, followed by Soxhlet extraction with methanol, acetone, hexane, and chloroform to remove the low molecular weight product. For the chlorobenzene fraction of each polymer, gel-permeation chromatography (GPC) analysis against polystyrene standard exhibited a number-averaged molecular mass (M_n) of 6.5 × 10^3 and 1.6 × 10^4 g mol^{-1} and a polydispersity (PDI) of 2.13 and 3.45 for **PIIG-DTBT** and **PIIG-DSeBT**, respectively. Note that the reported M_n and the PDI by using room-temperature GPC (THF as the eluent) only represented the soluble portion of each sample because each polymer was poorly soluble in THF.

Optical and electrochemical properties as well as theoretical calculations

The UV-Vis spectra of **PIIG-DTBT** and **PIIG-DSeBT** in chloroform solution and in solid state on the quartz are shown in Fig. 2a. The spectroscopic data of the polymers are summarized in Table 1. In both solution and films, the UV-Vis absorption spectra of the two polymers are similar in shape, exhibiting a broad band covering the whole visible region. Compared to their absorption spectra in solution, the broader absorption spectra in the solid state indicate that there are aggregations and/or orderly π–π stacking formed, which is beneficial for improving the charge mobility of the resulting films.

It is apparent that the absorption features of **PIIG-DSeBT** are obviously red-shifted relative to those of **PIIG-DTBT**. Thereby, the optical bandgap (E_g^{opt}) estimated from the absorption onset edge of the **PIIG-DSeBT** film is 1.46 eV, 150 meV smaller than that of **PIIG-DTBT** (1.61 eV), demonstrating that, in agreement with earlier studies,[34] the replacement of thiophene with selenophene in the polymer backbone results in both a red-shift of maximum

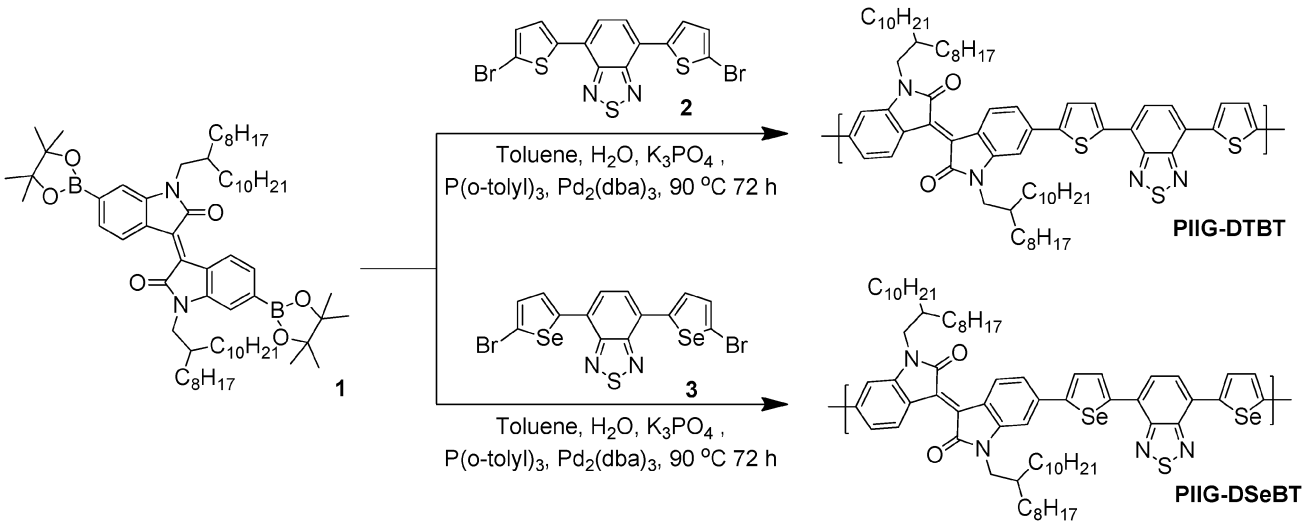

Scheme 1 Synthesis of **PIIG-DTBT** and **PIIG-DSeBT**.

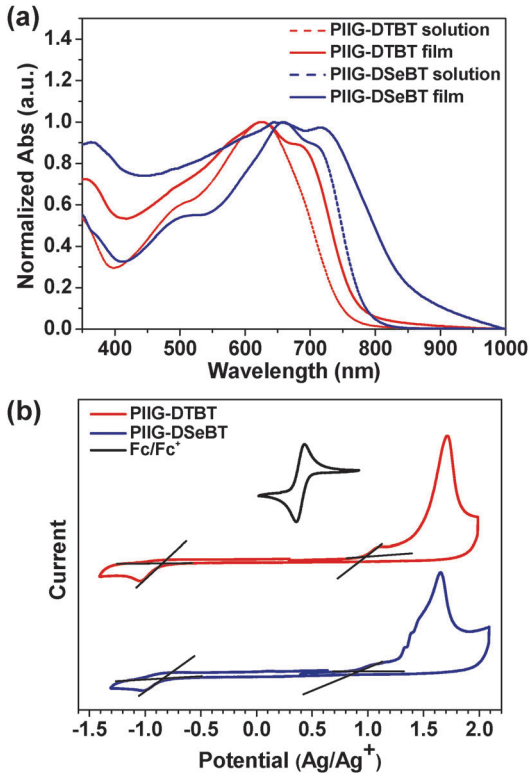

Fig. 2 (a) Normalized solution and film absorption spectra and (b) cyclic voltammograms of **PIIG-DTBT** and **PIIG-DSeBT**.

Table 1 UV-Vis absorption and electrochemical properties of the polymers

	λ_{max} (nm)	λ_{edge} (nm)	$E_g^{opt\,a}$ (eV)	$E_{HOMO}{}^{b}$ (eV)	$E_{LUMO}{}^{b}$ (eV)	$E_g^{elec\,c}$ (eV)
PIIG-DTBT	626	768	1.61	−5.39	−3.57	1.82
PIIG-DSeBT	667	851	1.46	−5.26	−3.57	1.69

[a] Calculated from the absorption band edge of the copolymer film, $E_g^{opt} = 1240/\lambda_{edge}$. [b] Thin films in 0.1 M $CH_3CN/n\text{-}Bu_4NPF_6$ *versus* ferrocenium/ferrocene at 50 mV s^{-1}. HOMO and LUMO estimated from the onset oxidation and reduction potentials, respectively, assuming the absolute energy level of ferrocene/ferrocenium to be 4.8 eV below vacuum. [c] E_g^{elec} (eV) = –(LUMO–HOMO).

absorbance and a reduction of optical bandgap. It is worth noting that, in comparison with PIIG-BT reported previously, the absorption maxima (λ_{max}) and onsets for both the polymers exhibit red-shifts, which is likely a result of the increase of the conjugation length and effective intramolecular charge transfer (ICT) after the insertion of electron-rich spacers (T or Se rings) along the backbones.

Cyclic voltammetry (CV) was performed to determine the energy levels of the polymers (Fig. 2b). The CV curves were recorded as referenced to an Ag/Ag^+ (0.1 M $n\text{-}Bu_4NPF_6$) electrode, which was calibrated by a ferrocene–ferrocenium (Fc/Fc^+) redox couple (4.8 eV below the vacuum level). The two polymers obviously display both p- and n-doping processes, in which their oxidative peaks are stronger than those of the reductive ones. The highest occupied molecular orbital (HOMO) and the

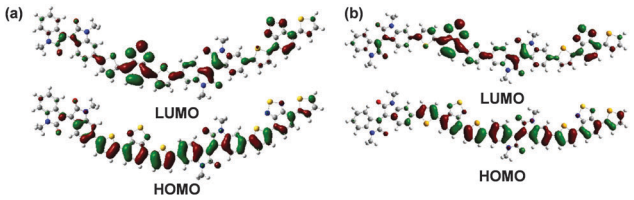

Fig. 3 DFT-optimized geometries and charge-density isosurfaces for the HOMO and LUMO levels of (a) $(\textbf{IIG-DTBT})_2$ and (b) $(\textbf{IIG-DSeBT})_2$ model systems.

lowest unoccupied molecular orbital (LUMO) energy levels are calculated to be −5.39/−3.57 eV for **PIIG-DTBT** and −5.26/−3.57 eV for **PIIG-DSeBT**, respectively. Compared with the energy levels of PIIG-BT (HOMO/LUMO = −5.68/−3.54 eV), both **PIIG-DTBT** and **PIIG-DSeBT** have significantly higher-lying HOMO levels, due to the presence of the electron-rich heteroaromatic units, whereas their LUMO levels remain almost unchanged. Besides, **PIIG-DSeBT** exhibits a 0.13 eV higher-lying HOMO level relative to **PIIG-DTBT**, indicating that the electron-donating strength of the Se spacer is stronger than that of the T unit. Thus, the calculated electrochemical bandgap (E_g^{elec}) of **PIIG-DSeBT** is smaller than that of **PIIG-DTBT**, which is consistent with the trend of E_g^{opt} deduced from the absorption onsets.

Distributions of HOMO and LUMO on the dimer systems of each polymer were calculated using the density functional theory (DFT) method at the B3LYP/6-31G level and are shown in Fig. 3. The computational results reveal that the HOMOs are well delocalized along the polymer chain, but the LUMOs are slightly localized on the BT core. This somewhat contrasts with many D–A IIG-based polymers, in which the LUMOs are almost spanned over the IIG unit. Therefore, we believe that the BT unit would have a slightly stronger electron affinity relative to IIG.

Thin-film microstructure analyses

The film morphologies of the IIG–BT polymers containing heteroaromatic spacers were investigated using tapping-mode atomic-force microscopy (AFM). The thin films were prepared on *n*-octadecyltrimethoxysilane (OTS)-treated SiO_2/Si substrates by the drop-casting method. As shown in Fig. 4, both polymers

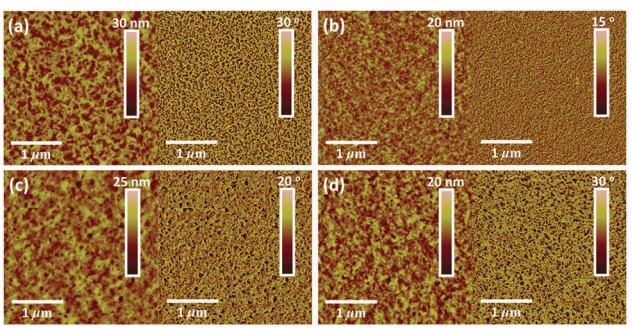

Fig. 4 AFM height (left) and phase (right) images of drop-cast polymer films of {(a) and (c)} **PIIG-DTBT** and {(b) and (d)} **PIIG-DSeBT**. {(a) and (b)} As-cast films and {(c) and (d)} annealed films at 220 °C on OTS-treated SiO_2/Si substrates.

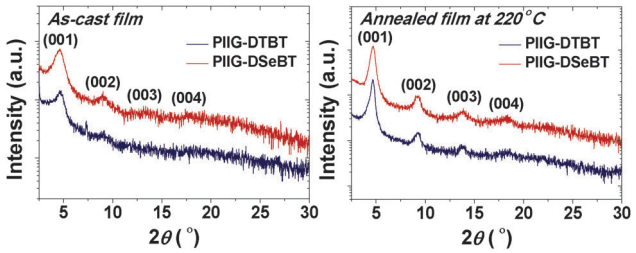

Fig. 5 Out-of-plane X-ray diffraction (XRD) patterns of **PIIG-DTBT** and **PIIG-DSeBT** thin films: as-cast film (left) and annealed film at 220 °C (right).

Table 2 Peak assignments for the out-of-plane XRD patterns obtained from **PIIG-DTBT** and **PIIG-DSeBT** thin films

Condition	(00*n*)	**PIIG-DTBT**		**PIIG-DSeBT**	
		2θ (°)	*d*(001)-spacing (Å)	2θ (°)	*d*(001)-spacing (Å)
As-cast film	(001)	4.63	19.07	4.58	19.28
	(002)	9.09	—	9.02	—
	(003)	—	—	13.53	—
	(004)	18.08	—	17.78	—
Annealed film at 220 °C	(001)	4.69	18.83	4.64	19.03
	(002)	9.29	—	9.24	—
	(003)	13.89	—	13.84	—
	(004)	18.34	—	18.28	—

formed densely packed nanofibrillar networks with the relatively smooth surface roughness of less than 3.2 nm. **PIIG-DTBT** films exhibited more distinct nanofibrillar structures compared to **PIIG-DSeBT** films. In addition, fibrillar aggregates with larger grains were observed from the polymer films thermally annealed at 220 °C for 30 min, which may indicate the formation of efficient pathways for charge-carrier transport after the thermal annealing. To further investigate the crystallinity and molecular orientations, X-ray diffraction (XRD) analysis was carried out on the IIG–BT polymer thin films (see Fig. 5). The spacer containing IIG–BT polymer thin films exhibited well-defined high order peaks up to (004), implying the formation of long-range lamellar packing in the thin films. **PIIG-DTBT** and **PIIG-DSeBT** films showed primary diffraction peaks at 2θ of 4.63° and 4.58°, respectively, which correspond to *d*(001)-spacing values of 19.07 Å and 19.28 Å, respectively (see Table 2). These are relatively reduced values compared to those of PIIG-BT (22.87 Å). This result demonstrates the positive effect of the heteroaromatic spacers on the dense molecular packing through the efficient donor–acceptor interaction between the polymer backbones. After annealing the polymer films, the diffraction peaks became remarkably stronger and more intensified, and the (001) layer distances were reduced to 18.83 Å and 19.03 Å for **PIIG-DTBT** and **PIIG-DSeBT**, respectively. These results are also indicative of the positive effects of the thermal annealing for the charge transport. The **PIIG-DTBT** thin film exhibited relatively denser crystalline natures than the **PIIG-DSeBT** thin film, which may lead to better electrical performance in **PIIG-DTBT** films (*vide infra*).

Organic field-effect transistors

In order to evaluate the electrical performance of the heteroaromatic spacer containing IIG–BT polymers, we fabricated bottom-gate/top-contact OFET devices. The polymer films were drop-cast onto OTS-treated SiO_2/Si substrates from an IIG-based

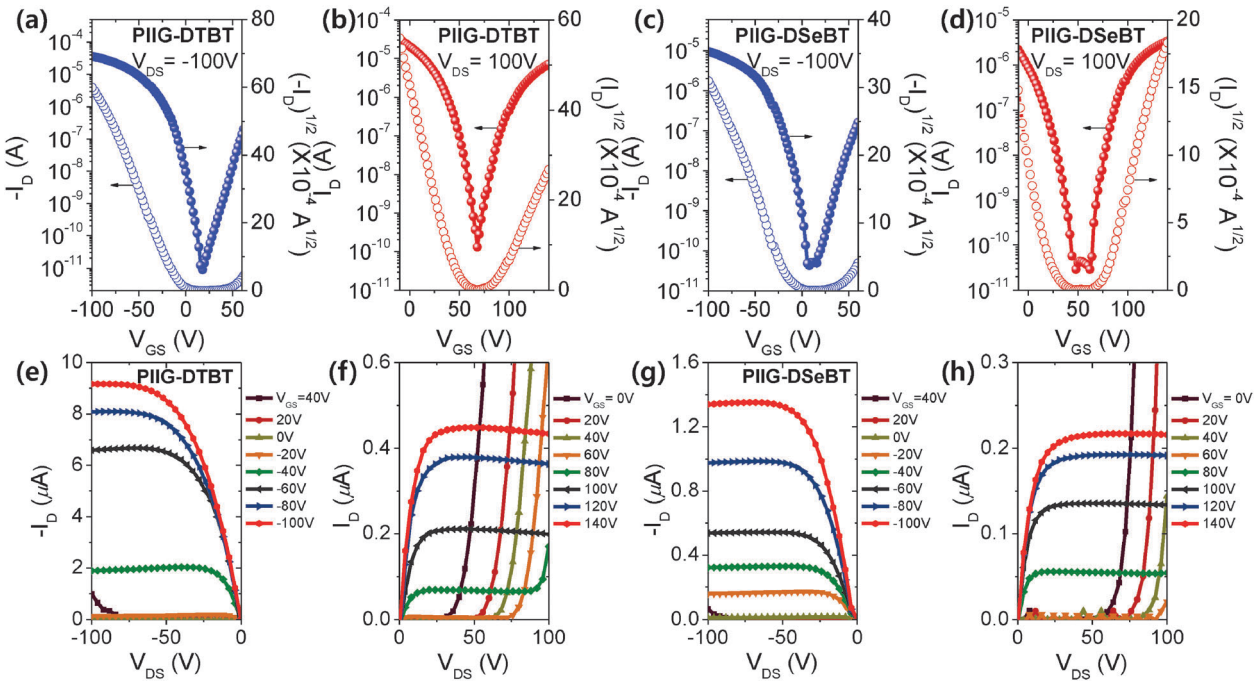

Fig. 6 FET characteristics obtained from spacer-containing IIG–BT polymer films annealed at 220 °C. Transfer curves of {(a) and (b)} **PIIG-DTBT** and {(c) and (d)} **PIIG-DSeBT** films at {(a) and (c)} hole- and {(b) and (d)} electron-enhancement operation with V_{DS} = −100 and +100 V, respectively. Output curves of {(e) and (f)} **PIIG-DTBT** and {(g) and (h)} **PIIG-DSeBT** films at {(e) and (g)} p- and {(f) and (h)} n-channel operation, respectively.

Table 3 OFET performance of spacer-containing IIG–BT polymer thin films

Polymer[a]	p-Channel				n-Channel			
	$\mu_{h,max}$[b] ($cm^2\ V^{-1}\ s^{-1}$)	$\mu_{h,avg}$[c] ($cm^2\ V^{-1}\ s^{-1}$)	I_{on}/I_{off}	V_T (V)	$\mu_{e,max}$ ($cm^2\ V^{-1}\ s^{-1}$)	$\mu_{e,avg}$ ($cm^2\ V^{-1}\ s^{-1}$)	I_{on}/I_{off}	V_T (V)
PIIG-DTBT	7.8×10^{-2}	4.3×10^{-2} ($\pm 1.9 \times 10^{-2}$)[d]	$>10^7$	−22.8	3.4×10^{-2}	1.4×10^{-2} ($\pm 1.3 \times 10^{-2}$)	$>10^5$	95.6
PIIG-DSeBT	2.6×10^{-2}	2.0×10^{-2} ($\pm 4.8 \times 10^{-3}$)	$>10^6$	−20.9	1.5×10^{-2}	5.3×10^{-3} ($\pm 4.2 \times 10^{-3}$)	$>10^4$	87.2

[a] The polymer films were annealed at 220 °C and the FET performance of more than 10 devices was tested in a nitrogen atmosphere. [b] The maximum and [c] average mobility of the FET devices (L = 50 μm and W = 1000 μm). [d] Standard deviation.

polymer solution in *o*-dichlorobenzene (3 mg mL^{-1}). Note that the solubility of **PIIG-DSeBT** was relatively poorer than that of **PIIG-DTBT**, thus heating the **PIIG-DSeBT** solution at a high temperature (more than 100 °C) was required to suppress the precipitation of the polymer during solution processing. For the heteroaromatic spacer inserted IIG-based polymer films, the annealed thin films exhibited significantly enhanced FET performance compared with the as-cast polymer thin films and the optimum thermal annealing temperature was found to be 220 °C (see Fig. S1 and Table S1, ESI†). Fig. 6 shows the representative *I–V* characteristics of transfer and output curves from the optimized FETs annealed at 220 °C and their electrical performances are summarized in Table 3. In contrast to the n-type electrical performance of PIIG-BT, both **PIIG-DTBT** and **PIIG-DSeBT** exhibited ambipolar characteristics, displaying typical V-shaped transfer curves. The ambipolar behaviors of **PIIG-DTBT** and **PIIG-DSeBT** can be mainly attributed to the smaller bandgaps induced by the extension of the conjugation length and the enhanced ICT of the spacer containing IIG–BT polymers. In particular, the energetically low-lying HOMO level of PIIG-BT prohibits the efficient injection of hole carriers with regard to the gold contact, whereas the higher-lying HOMO levels of **PIIG-DTBT** and **PIIG-DSeBT** allow more efficient injection of hole carriers relative to the gold contact, thereby leading to more pronounced ambipolar behaviors. The higher ambipolar FET performance was observed in the annealed **PIIG-DTBT** films ($\mu_{h,max}$ and $\mu_{e,max}$ of 7.8×10^{-2} and 3.4×10^{-2} $cm^2\ V^{-1}\ s^{-1}$, respectively), which is most likely due to their optimized thin film microstructures compared to **PIIG-DSeBT** films ($\mu_{h,max}$ = 2.6×10^{-2} $cm^2\ V^{-1}\ s^{-1}$ and $\mu_{e,max}$ = 1.5×10^{-2} $cm^2\ V^{-1}\ s^{-1}$). The slightly hole-dominant charge transport in their ambipolar characteristics is presumably due to the relatively smaller injection barriers for holes with respect to the gold contacts as well as to the delocalization of HOMO orbitals. In addition, the threshold voltages (V_T) of **PIIG-DSeBT** were slightly smaller than **PIIG-DTBT**, owing to its easy turn-on characteristics induced by the lower bandgap. The complementary metal–oxide–semiconductor (CMOS)-like inverter characteristics of **PIIG-DTBT** and **PIIG-DSeBT** were also investigated using two identical ambipolar transistors. Output voltage (V_{OUT}) was monitored as a function of input voltage (V_{IN}) at a constant supply bias (V_{DD}). The voltage transfer characteristic (VTC) curves are shown in Fig. S2 (ESI†), and high gains of 36.2 and 21.6 were obtained from **PIIG-DTBT** and **PIIG-DSeBT**, respectively. Although the asymmetry in mobility and threshold voltage in p- and n-channel modes should be complemented by further optimization of device architecture for both polymers, **PIIG-DTBT** exhibited a relatively high gain because of the better ambipolar charge-carrier mobilities.

Conclusions

Two new polymeric hybrids (**PIIG-DTBT** and **PIIG-DSeBT**) containing IIG, BT, and five-membered heteroaromatic spacers (T and Se) were synthesized and characterized, and their OFET performance was evaluated with the goal of attaining an understanding of the effect of the insertion of the spacers. Compared to the PIIG-BT polymer directly incorporating IIG or BT units in the main backbone, the presence of the spacers regularly inserted into the polymeric backbones caused a red-shift, resulting in relatively narrow energy bandgaps. This is mainly attributed to the extended conjugation length and enhanced ICT. Both the polymers formed a well-ordered lamellar structure with fibrillar grains in the thin film. Besides the fine-tuning of optical properties and energy levels afforded by the simple structural modifications described in this study, the heteroaromatic spacers endowed both polymers with changed polarity in OFET devices, resulting in relatively well-balanced ambipolar transport, and for **PIIG-DTBT**, the hole and electron mobilities as high as 7.8×10^{-2} and 3.4×10^{-2} $cm^2\ V^{-1}\ s^{-1}$ were achieved. To the best of our knowledge, this is the second example of IIG-based polymers presenting ambipolar characteristics in OFETs reported to date.

Acknowledgements

This work was supported by the National Research Foundation of Korea (NRF) funded by the Ministry of Education (2013-R1A1A1A05004475, 10Z20130011057 (BK21), 2014R1A2A2A01007467), Global Frontier Research Program of Ministry of Science, ICT and Future Planning (2013M3A6A5073175).

Notes and references

1 C. Wang, H. Dong, W. Hu, Y. Liu and D. Zhu, *Chem. Rev.*, 2011, **112**, 2208.
2 J. Rivnay, L. H. Jimison, J. E. Northrup, M. F. Toney, R. Noriega, S. Lu, T. J. Marks, A. Facchetti and A. Salleo, *Nat. Mater.*, 2009, **8**, 952.
3 P. M. Beaujuge and J. M. Fréchet, *J. Am. Chem. Soc.*, 2011, **133**, 20009.
4 G. Giri, E. Verploegen, S. C. Mannsfeld, S. Atahan-Evrenk, D. H. Kim, S. Y. Lee, H. A. Becerril, A. Aspuru-Guzik, M. F. Toney and Z. Bao, *Nature*, 2011, **480**, 504.

5 H. Sirringhaus, *Adv. Mater.*, 2005, **17**, 2411.
6 I. McCulloch, M. Heeney, C. Bailey, K. Genevicius, I. MacDonald, M. Shkunov, D. Sparrowe, S. Tierney, R. Wagner, W. Zhang, M. L. Chabinyc, R. J. Kline, M. D. McGehee and M. F. Toney, *Nat. Mater.*, 2006, **5**, 328.
7 H. E. Katz, *Chem. Mater.*, 2004, **16**, 4748.
8 E. Meijer, D. De Leeuw, S. Setayesh, E. Van Veenendaal, B.-H. Huisman, P. Blom, J. Hummelen, U. Scherf and T. Klapwijk, *Nat. Mater.*, 2003, **2**, 678.
9 F. Garnier, R. Hajlaoui, A. Yassar and P. Srivastava, *Science*, 1994, **265**, 1684.
10 X. Guo, M. Baumgarten and K. Müllen, *Prog. Polym. Sci.*, 2013, **38**, 1832.
11 J. Lee, A.-R. Han, J. Kim, Y. Kim, J. H. Oh and C. Yang, *J. Am. Chem. Soc.*, 2012, **134**, 20713.
12 J. Lee, A.-R. Han, H. Yu, T. J. Shin, C. Yang and J. H. Oh, *J. Am. Chem. Soc.*, 2013, **135**, 9540.
13 J. Zaumseil and H. Sirringhaus, *Chem. Rev.*, 2007, **107**, 1296.
14 D. Cortizo-Lacalle, S. Arumugam, S. E. Elmasly, A. L. Kanibolotsky, N. J. Findlay, A. R. Inigo and P. J. Skabara, *J. Mater. Chem.*, 2012, **22**, 11310.
15 R. Schmidt, J. H. Oh, Y.-S. Sun, M. Deppisch, A.-M. Krause, K. Radacki, H. Braunschweig, M. Könemann, P. Erk and Z. Bao, *J. Am. Chem. Soc.*, 2009, **131**, 6215.
16 Y. Kim, J. Hong, J. H. Oh and C. Yang, *Chem. Mater.*, 2013, **25**, 3251.
17 J. Kim, A.-R. Han, J. H. Seo, J. H. Oh and C. Yang, *Chem. Mater.*, 2012, **24**, 3464.
18 J. Lee, S. Cho, J. H. Seo, P. Anant, J. Jacob and C. Yang, *J. Mater. Chem.*, 2012, **22**, 1504.
19 S.-L. Suraru, U. Zschieschang, H. Klauk and F. Würthner, *Chem. Commun.*, 2011, **47**, 1767.
20 R. Stalder, J. Mei, J. Subbiah, C. Grand, L. A. Estrada, F. So and J. R. Reynolds, *Macromolecules*, 2011, **44**, 6303.
21 J. Mei, K. R. Graham, R. Stalder and J. R. Reynolds, *Org. Lett.*, 2010, **12**, 660.
22 G. Kim, A.-R. Han, H. R. Lee, J. Lee, J. H. Oh and C. Yang, *Chem. Commun.*, 2014, **50**, 2180.
23 F. Grenier, P. Berrouard, J.-R. Pouliot, H.-R. Tseng, A. J. Heeger and M. Leclerc, *Polym. Chem.*, 2013, **4**, 1836.
24 E. Wang, W. Mammo and M. R. Andersson, *Adv. Mater.*, 2014, **26**, 1801.
25 T. Lei, Y. Cao, Y. Fan, C.-J. Liu, S.-C. Yuan and J. Pei, *J. Am. Chem. Soc.*, 2011, **133**, 6099.
26 T. Lei, Y. Cao, X. Zhou, Y. Peng, J. Bian and J. Pei, *Chem. Mater.*, 2012, **24**, 1762.
27 J. Mei, D. H. Kim, A. L. Ayzner, M. F. Toney and Z. Bao, *J. Am. Chem. Soc.*, 2011, **133**, 20130.
28 T. Lei, J. H. Dou and J. Pei, *Adv. Mater.*, 2012, **24**, 6457.
29 T. Lei, J.-H. Dou, Z.-J. Ma, C.-H. Yao, C.-J. Liu, J.-Y. Wang and J. Pei, *J. Am. Chem. Soc.*, 2012, **134**, 20025.
30 A. J. Kronemeijer, E. Gili, M. Shahid, J. Rivnay, A. Salleo, M. Heeney and H. Sirringhaus, *Adv. Mater.*, 2012, **24**, 1558.
31 M. Shahid, R. S. Ashraf, Z. Huang, A. J. Kronemeijer, T. McCarthy-Ward, I. McCulloch, J. R. Durrant, H. Sirringhaus and M. Heeney, *J. Mater. Chem.*, 2012, **22**, 12817.
32 H. Sirringhaus, P. Brown, R. Friend, M. M. Nielsen, K. Bechgaard, B. Langeveld-Voss, A. Spiering, R. A. Janssen, E. Meijer and P. Herwig, *Nature*, 1999, **401**, 685.
33 G. Kim, H. R. Yeom, S. Cho, J. H. Seo, J. Y. Kim and C. Yang, *Macromolecules*, 2012, **45**, 1847.
34 B. Kim, H. R. Yeom, M. H. Yun, J. Y. Kim and C. Yang, *Macromolecules*, 2012, **45**, 8658.
35 Y. Ito, A. A. Virkar, S. Mannsfeld, J. H. Oh, M. Toney, J. Locklin and Z. Bao, *J. Am. Chem. Soc.*, 2009, **131**, 9396.